

# Mouse genetic background impacts susceptibility to hyperoxia-driven perturbations to lung maturation

Jennifer Tiono<sup>1,2</sup> | David E Surate Solaligue<sup>1,2</sup> | Ivana Mižiková<sup>1,2</sup> |  
 Claudio Nardiello<sup>1,2</sup> | István Vadász<sup>2</sup> | Eva Böttcher-Friebertshäuser<sup>3</sup> |  
 Harald Ehrhardt<sup>4</sup> | Susanne Herold<sup>2</sup> | Werner Seeger<sup>1,2</sup> | Rory E Morty<sup>1,2</sup> 

<sup>1</sup>Department of Lung Development and Remodelling, Max Planck Institute for Heart and Lung Research, member of the German Center for Lung Research (DZL), Bad Nauheim, Germany

<sup>2</sup>Department of Internal Medicine (Pulmonology), Universities of Giessen and Marburg Lung Center, member of The German Center for Lung Research (DZL), Giessen, Germany

<sup>3</sup>Institute of Virology, Philipps University Marburg, Marburg, Germany

<sup>4</sup>Division of General Pediatrics and Neonatology, University Children's Hospital Giessen, Justus Liebig, University, Giessen, Germany

## Correspondence

Rory E Morty, Department of Lung Development and Remodelling, Max Planck Institute for Heart and Lung Research, Parkstrasse 1, D-61231 Bad Nauheim, Germany.  
 Email: rory.morty@mpi-bn.mpg.de

## Funding information

Max-Planck-Gesellschaft, Grant/Award Number: HLR; Deutsche Forschungsgemeinschaft, Grant/Award Numbers: 1789/1, KFO309, SFB1213, EXC147; Hessisches Ministerium für Wissenschaft und Kunst, Grant/Award Number: UGMLC-LOEWE; University Hospital Giessen and Marburg, Grant/Award Number: UKGM62589135

## Abstract

**Background:** The laboratory mouse is widely used in preclinical models of bronchopulmonary dysplasia, where lung alveolarization is stunted by exposure of pups to hyperoxia. Whether the diverse genetic backgrounds of different inbred mouse strains impacts lung development in newborn mice exposed to hyperoxia has not been systematically assessed.

**Methods:** Hyperoxia (85% O<sub>2</sub>, 14 days)-induced perturbations to lung alveolarization were assessed by design-based stereology in C57BL/6J, BALB/cJ, FVB/NJ, C3H/HeJ, and DBA/2J inbred mouse strains. The expression of components of the lung antioxidant machinery was assessed by real-time reverse transcriptase polymerase chain reaction and immunoblot.

**Results:** Hyperoxia-reduced lung alveolar density in all five mouse strains to different degrees (C57BL/6J, 64.8%; FVB/NJ, 47.4%; BALB/cJ, 46.4%; DBA/2J, 45.9%; and C3H/HeJ, 35.9%). Hyperoxia caused a 94.5% increase in mean linear intercept in the C57BL/6J strain, whilst the C3H/HeJ strain was the least affected (31.6% increase). In contrast, hyperoxia caused a 65.4% increase in septal thickness in the FVB/NJ strain, where the C57BL/6J strain was the least affected (30.3% increase). The expression of components of the lung antioxidant machinery in response to hyperoxia was strain dependent, with the C57BL/6J strain exhibiting the most dramatic engagement. Baseline expression levels of components of the lung antioxidant systems were different in the five mouse strains studied, under both normoxic and hyperoxic conditions.

**Conclusion:** The genetic background of laboratory mouse strains dramatically influenced the response of the developing lung to hyperoxic insult. This might be explained, at least in part, by differences in how antioxidant systems are engaged by different mouse strains after hyperoxia exposure.

## KEYWORDS

alveolarization, bronchopulmonary dysplasia, hyperoxia, strain

## 1 | BACKGROUND

Bronchopulmonary dysplasia (BPD) remains a common and serious complication of preterm birth. While first described in 1967,<sup>1</sup> both patient demographics and the histopathological picture of BPD have changed over time.<sup>2,3</sup> Today, BPD is more prevalent in the most preterm born infants (<28 weeks of gestational age),<sup>4</sup> and BPD lung histopathology largely reflect stunting of lung alveolarization and aberrant lung vascular development.<sup>5</sup> These histopathological hallmarks of BPD arise from a combination of oxygen toxicity and oxidative stress,<sup>6–8</sup> where infants receive oxygen supplementation to manage acute respiratory failure; as well as baro- and volutrauma from mechanical intervention, which may be required to manage the most severely affected patients.<sup>5</sup> Antenatal factors,<sup>9–11</sup> infection and inflammation,<sup>12</sup> and genetic predisposition<sup>13</sup> have also been proposed as contributors to BPD pathogenesis.<sup>5,14</sup> The persistence of BPD in a neonatal intensive care setting has underscored a pressing need for advances in our understanding of the pathomechanisms at play in affected patients. Such studies are generally undertaken in animal models, utilizing primarily term-born mouse and rat pups,<sup>15</sup> although available models extend to nonhuman primates.<sup>16</sup>

The term-born mouse<sup>17</sup> and rat<sup>18</sup> models of BPD employ a variety of stimuli to generate the stunted lung development seen in patients with BPD,<sup>19</sup> including elevated oxygen levels and/or mechanical ventilation<sup>20</sup>; sometimes combined with a second insult, such as antenatal or intrauterine bacterial lipopolysaccharide to mimic a background of chorioamnionitis.<sup>19</sup> Elevated oxygen levels are the most widely used injurious stimuli in BPD models, and the impact of the degree of oxygen toxicity and the window of oxygen exposure on postnatal lung alveolarization continue to be evaluated.<sup>21</sup>

The role of the mouse and rat strains selected for preclinical modeling of BPD has long been neglected as a potentially important variable in studies on postnatal lung maturation. A spectrum of mouse strains is currently used in studies on BPD, including C57BL/6, BALB/c, A/J, C3H/He, FVB/N, and DBA/2 inbred strains. That different strains are widely used is important, because both strain-independent and strain-dependent patterns of gene expression have been noted in the lungs of C57BL/6J, A/J, and C3H/HeJ strains in a genome-wide analysis of 26 time-points between embryonic day (E) 9.5 and postnatal day (P)56.<sup>22</sup> Thus, the dynamics of gene expression during lung development can be strain dependent. In addition, mouse genetic background has been documented to play a role in determining the degree of lung inflammation provoked by exposure of newborn mouse pups from 36 inbred mouse strains to hyperoxia,<sup>23</sup> a process in which *Nrf2* has been implicated.<sup>24</sup> A similar strain-dependent inflammatory response had also been noted in adult mice from six<sup>25</sup> and nine<sup>26</sup> inbred strains exposed to hyperoxia. These concerns extend to substrains, given demonstrable differences in responses of the retina to 75% O<sub>2</sub> over the period P1 to P14, comparing C57BL/6J and C57BL/6N mouse pups.<sup>27</sup>

The issue of inbred mouse strain in studies on lung development and BPD are also beginning to emerge, with one recent report highlighting that pharmacological intervention with the thioredoxin

reductase-1 inhibitor aurothioglucose prevented the deleterious effects of hyperoxia exposure on lung alveolarization in C3H/HeN mouse pups, but not in C57BL/6 mouse pups.<sup>28</sup> These reports highlight that consideration of the mouse strain used in preclinical studies on BPD pathogenesis is essential for data interpretation, and for the comparison of experimental outcomes reported in different mouse strains in the literature. However, no study has provided a side-by-side comparison of how lung alveolarization in inbred mouse strains responds to oxygen toxicity. To this end, we present here a side-by-side comparison of lung alveolarization and the gene expression of key mediators of the lung antioxidant response, in five different inbred mouse strains: C57BL/6J, BALB/cJ, FVB/NJ, C3H/HeJ, and DBA/2J. These data support the use of specific mouse strains in the study of hyperoxia-induced perturbations to postnatal lung maturation and hyperoxia-driven engagement of redox management pathways in the lung.

## 2 | OBJECTIVE

The objective of this study was to assess whether the genetic background of five different mouse strains—C57BL/6J, BALB/cJ, FVB/NJ, C3H/HeJ, and DBA/2J inbred strains—impacted the effect of hyperoxia exposure on lung alveolarization and gene expression of key mediators of the lung antioxidant response.

## 3 | METHODS

### 3.1 | Animal studies

All animal procedures were approved by the local authorities, the *Regierungspräsidium Darmstadt* (approval B2/1108), which houses the equivalent of an Institutional Animal Care and Use Committee in Germany. The C57BL/6J, BALB/cJ, FVB/NJ, C3H/HeJ, and DBA/2J mouse strains were purchased from The Jackson Laboratory (Bar Harbor, MA). The 129S2/SvPasOrIRj mouse strain was purchased from Janvier (Le Genest-Saint-Isle, France).

Newborn mouse pups of all strains were randomized to litter sizes of either four or five, which are smaller than the litter sizes generally used (a litter size of six is generally used by the investigators for studies on C57BL/6J mice<sup>21,29,30</sup>), however, were used to match the smaller litter sizes of the DBA/2J mouse strain. Mouse pups were exposed to normoxic (21% O<sub>2</sub>) or hyperoxic (85% O<sub>2</sub>) conditions from the day of birth (designated P1) to the 14th day of postnatal life (P14), in a well-established experimental animal model of BPD using the Pro-Ox oxygen control and delivery system of BioSpherix (Parish, NY).<sup>21</sup> Litter sizes were matched at the same number, for corresponding normoxia and hyperoxia exposures of pups of the same strain. Nursing dams were rotated every 24 hours between normoxia- and hyperoxia-exposed litters, to avoid oxygen toxicity. Dams and pups were maintained on a 12/12-hour light-dark cycle and received food ad libitum. Mouse pups were killed on day P14 by pentobarbital overdose (500 mg/kg, intraperitoneal).

### 3.2 | Design-based stereology

Lung structure analyses were based on the American Thoracic Society/European Respiratory Society recommendations.<sup>31</sup> The design-based stereology approach has been described previously.<sup>32,33</sup> After sternotomy, mouse lungs were fixed by intratracheal instillation of 1.5% (mass/vol) paraformaldehyde, 1.5% (mass/vol) glutaraldehyde in 150 mM 4-(2-hydroxyethyl)-1-piperazineethanesulfonic acid, pH 7.4, for 24 hours at 4°C, at a hydrostatic pressure of 20 cm H<sub>2</sub>O.

Lung tissue blocks were collected according to the systematic uniform random sampling.<sup>34</sup> Lungs were embedded in toto in 2% (mass/vol) agar-agar, and sectioned at 3 mm, and lung volume was assessed by Cavalieri's principle.<sup>35</sup> Lungs embedded in agar-agar were treated with 1% (mass/vol) osmium tetroxide (8371.3; Roth, Karlsruhe, Germany) in 0.1 M sodium cacodylate (15540.03; Serva, Heidelberg, Germany), and 2.5% (mass/vol) uranyl acetate (77870.01; Serva, Darmstadt, Germany) in double-distilled water; and embedded in glycol methacrylate (Technovit 7100; 64709003; Heraeus Kulzer, Hanau, Germany). Blocks were sectioned exhaustively at 2 μm, and every first and third section of a consecutive series was stained with Richardson's stain,<sup>36</sup> for determination of the total number of alveoli and alveolar density. Sections were collected for analysis of all other stereological parameters by collecting every tenth section of a consecutive series in the same Technovit block, which was stained with Richardson's stain. Images of tissue sections were captured with a NanoZoomer-XR C12000 Digital slide scanner (Hamamatsu Photonics Deutschland, Herrsching am Ammersee, Germany).

Digital tissue sections were analyzed with the Visiopharm newCAST computer-assisted stereology system (VIS 4.5.3). Analyses included determination of mean linear intercept (MLI), arithmetic mean septal thickness, and total alveoli number. The coefficient of error (CE), the coefficient of variation (CV), and the squared ratio between both (CE<sup>2</sup>/CV<sup>2</sup>) were calculated, where CE<sup>2</sup>/CV<sup>2</sup> < 0.5 validated precision of the measurements.

### 3.3 | Messenger RNA expression analysis

Steady-state messenger RNA (mRNA) levels were assessed in total RNA pools isolated from mouse lungs as described previously.<sup>37</sup> Steady-state mRNA levels were determined by real-time reverse transcriptase polymerase chain reaction (real-time RT-PCR) as described previously,<sup>37</sup> using the primers listed in Table 1, where *Polr2a* served as a reference gene. The real-time RT-PCR data are presented as the difference in cycle threshold (C<sub>t</sub>), ΔC<sub>t</sub>, which reflects the C<sub>t</sub> (*Polr2a*) - C<sub>t</sub> (*gene of interest*). Fold change in mRNA abundance was given by fold change = 2<sup>ΔΔC<sub>t</sub></sup>.

### 3.4 | Protein expression analysis

Steady-state protein levels were documented by immunoblot, undertaken as described previously.<sup>37</sup> Antigens were detected with mouse anti-superoxide dismutase 3 (SOD3; #ab80946; 1:1000;

Abcam, Berlin) and rabbit anti-glutathione synthetase (GSS; #ab133592; 1:1000; Abcam, Berlin). The detection of a single well-resolved band for target proteins of interested is presented in uncropped immunoblots for SOD3 (Figure S1A) and GSS (Figure S1B). Loading equivalence was documented with a rabbit anti-mouse β-actin antibody (#4967; 1:1000; Cell Signaling Technology, Frankfurt am Main). Immune complexes were detected with either goat anti-mouse IgG(H+L)-horseradish peroxidase (HRPO) conjugate (#31430; 1:5000; Thermo Fisher Scientific, Karlsruhe) or goat anti-rabbit IgG(H+L)-HRPO conjugate (#31460; 1:2000; Thermo Fisher Scientific, Karlsruhe).

### 3.5 | Sex genotyping

Sexes of mice were determined by screening for the male-specific *SRY* locus and the sex-independent *I13* gene, exactly as described previously.<sup>38</sup>

### 3.6 | Statistics

Data are presented in scatter plots as mean ± SD. Two-group comparisons were made by the unpaired Student *t* test. All statistical analyses were performed with the GraphPad Prism 6.0. Statistical outliers were screened for using the Grubbs test, and none were found.

## 4 | RESULTS

### 4.1 | Five of six mouse strains survived hyperoxia exposure

Six mouse strains were tested for tolerance to hyperoxia. The mouse strains were selected to provide as diverse a strain background as possible, as illustrated in Figure 1A; where a mouse strain family tree based on 1638 informative single-nucleotide polymorphisms compared in 106 inbred mouse strains<sup>39</sup> demonstrated the genetic relatedness of the six mouse strains investigated. Of the six mouse strains investigated, the C57BL/6J, BALB/cJ, FVB/NJ, C3H/HeJ, and DBA/2J strains survived exposure to 85% O<sub>2</sub> over the first 14 days of postnatal life, with overall survival rates of 100% (C57BL/6J and BALB/cJ), 89% (FVB/NJ), 78% (C3H/HeJ), and 67% (DBA/2J; Figure 1B). In these cases, no morbidity was observed in mouse pups, and mortality was scored when a mouse pup was found dead in the cage. The 129S2/SvPasOrlRj strain did not tolerate hyperoxia, with loss of the entire litter within 4 days, in multiple experimental runs.

### 4.2 | Hyperoxia effects on lung architecture are strain dependent

Visual inspection of the Richardson-stained, plastic-embedded lung tissue sections suggested that the mean diameter of an alveolus was larger in normoxia-exposed C3H/HeJ mouse pups compared with the other mouse strains used (Figure 2). Hyperoxia caused a visible increase in the size of alveoli, as assessed by visual inspection of lung

**TABLE 1** Primers used for real-time RT-PCR analysis.

Genes	Primers	Primer sequences, 5'-3'	Amplicon size, bp	T <sub>m</sub> , °C	Location, bp
<i>Txn1</i>	Forward	GGGAGTTCTCCGGTGCTAAC	128	61.4	459-478
	Reverse	AGCAGTGGCTTAGGGGACTA		59.4	586-565
<i>Sod1</i>	Forward	GTCGGCTTCTCGTCTTGCTC	155	61.4	701-720
	Reverse	CCCATGCTGGCCTTCAGTTA		59.4	855-836
<i>Sod2</i>	Forward	GCCTGCTTAATCAGGACCC	138	61.4	1386-1405
	Reverse	AGACTACAGCACCCAGTCA		59.4	1523-1504
<i>Sod3</i>	Forward	CCTTCTGTCTACGGCTTGC	117	59.8	93-113
	Reverse	TCGCCTATCTTCTCAACCAGG		59.4	209-118
<i>Cat</i>	Forward	ACCGTGCTCTGTGCATCTTAT	125	57.9	91-113
	Reverse	GGAAGCCCTACAGGAAAAACT		60.3	215-193
<i>Nfe2l2</i>	Forward	CAGAGTGATGGTTGCCACT	154	59.4	102-121
	Reverse	GACACTGGTCACACTGGGT		59.4	255-234
<i>Gpx</i>	Forward	AGTCCACCGTGTATGCCTTCT	124	59.8	830-849
	Reverse	GAGACGCGACATTCTCAATGA		57.9	953-934
<i>Gsr</i>	Forward	GACACCTCTTCCTTCGACTACC	117	62.1	1302-1322
	Reverse	CCCAGCTTGTGACTCTCCAC		61.4	1418-1397
<i>Gss</i>	Forward	CAAAGCAGCCATAGACAGGG	138	61.8	1386-1405
	Reverse	AAAAGCGTGAATGGGCATAC		57.9	1523-1504
<i>Txnrd1</i>	Forward	CATTGAAGGAGAAGCCCTGGT	117	52.4	93-113
	Reverse	GAGGGCAGATACAGGGGTCA		61.4	209-118
<i>Txnrd2</i>	Forward	GATCCGGTGGCCTAGCTTG	125	61.0	91-113
	Reverse	TCGGGGAGAAGGTTCACAT		59.4	215-193
<i>Prdx1</i>	Forward	GTCTGAGCTGTGTTTTGGGC	154	59.4	102-121
	Reverse	ATGGTACACATGCTGGGGAAA		57.9	255-234
<i>Prdx2</i>	Forward	CACCTGGCGTGGATCAATACC	124	61.8	830-849
	Reverse	GACCCCTGTAAGCAATGCC		61.4	953-934
<i>Prdx3</i>	Forward	GGTTGCTCGTCATGCAAGTG	155	59.4	701-720
	Reverse	CCACAGTATGTCTGTCAACAGG		60.6	855-836
<i>Prdx4</i>	Forward	TCCTGTTGCGGACCGAATC	138	58.8	1386-1405
	Reverse	CCACCAGCGTAGAAGTGGC		61.0	1523-1504
<i>Prdx5</i>	Forward	GGCTGTTCTAAGACCCACCTG	117	61.8	93-113
	Reverse	GGAGCCGAACCTTGCCCTTC		61.0	209-118
<i>Prdx6</i>	Forward	CGCCAGAGTTTGCCAAGAG	125	58.8	91-113
	Reverse	TCCGTGGGTGTTTCACCATTG		59.8	215-193
<i>Pon1</i>	Forward	CGGAAGGGAGAACAGTGCAA	154	59.4	102-121
	Reverse	CAGGTCGGCTACAATATCGTC		59.8	255-234
<i>Pon2</i>	Forward	AGGAATCGAAACTGGAGCTGA	124	57.9	830-849
	Reverse	AGTGCTAATGCCATGTGGGT		57.3	953-934
<i>Pon3</i>	Forward	GCACCGTGGCTTCTGTGTAT	117	59.4	1302-1322
	Reverse	GGGTGTTGGGCACATACAGT		59.4	1418-1397
<i>Hmox1</i>	Forward	AAATGCAATACTGGCCCCCA	117	57.3	1302-1322
	Reverse	ACAGCTGCTTTTACAGGCCA		57.3	1418-1397
<i>Polr2a</i>	Forward	CTAAGGGGCAGCCAAAGAAAC	209	59.5	808-828
	Reverse	CCATTCAGCATACAACCTAGGC		59.2	1016-994

Abbreviations: bp, base pair; real-time RT-PCR, real-time reverse transcriptase polymerase chain reaction

tissue sections with the magnitude of the enlargement of alveoli (caused by hyperoxia exposure) being apparently greater in the C57BL/6J, BALB/cJ, and FVB/NJ strains, and smaller in the C3H/HeJ and DBA/2J strains.

Design-based stereology was used to quantify changes in lung architecture, where hyperoxia caused the most dramatic reduction in alveoli number in C57BL/6J mouse pups (74.5%; Figure 3A). Smaller magnitude decreases in total alveoli number were noted in other strains

**TABLE 2** Structural parameters assessed for the lungs of mouse pups exposed to 21% O<sub>2</sub> normoxia for the first 14 days of postnatal life

Parameter	C57BL/6J mean (SD)	BALB/cJ mean (SD)	FVB/NJ mean (SD)	C3H/HeJ mean (SD)	DBA/2J mean (SD)
V (lung) [cm <sup>3</sup> ]	0.3631 (0.05834)	0.2641 (0.0708)	0.2432 (0.03140)	0.3142 (0.07904)	0.2414 (0.07284)
CE CV	0.072 0.160 0.200	0.120 0.268 0.200	0.058 0.129 0.200	0.113 0.251 0.200	0.135 0.3017 0.200
V <sub>v</sub> (par/lung) [%]	0.9328 (0.0051)	0.9377 (0.0220)	0.9441 (0.0306)	0.8986 (0.0124)	0.9326 (0.0415)
CE CV	0.003 0.005 0.250	0.010 0.023 0.200	0.014 0.032 0.200	0.006 0.014 0.200	0.020 0.045 0.250
N (alv, lung) 10 <sup>6</sup>	5.01 (0.719)	4.31 (1.000)	3.65 (0.444)	3.51 (0.907)	2.89 (0.656)
CE CV	0.064 0.143 0.201	0.104 0.232 0.202	0.055 0.121 0.201	0.116 0.258 0.200	0.101 0.226 0.199
N <sub>v</sub> (alv/par, lung) 10 <sup>7</sup> [cm <sup>-3</sup> ]	1.508 (0.2383)	1.764 (0.2053)	1.594 (0.1091)	1.249 (0.1785)	1.231 (0.3649)
CE CV	0.071 0.158 0.200	0.052 0.116 0.200	0.031 0.068 0.200	0.064 0.143 0.200	0.133 0.296 0.200
S <sub>v</sub> (lung) [cm <sup>-1</sup> ]	804 (46.73)	888.8 (51.47)	869.1 (70.47)	634.2 (42.38)	774.2 (66.86)
CE CV	0.026 0.058 0.200	0.026 0.058 0.200	0.036 0.081 0.200	0.030 0.067 0.200	0.039 0.086 0.200
S (alv epi, lung) [cm <sup>2</sup> ]	269.0 (34.94)	219.2 (55.07)	199.2 (27.98)	178.2 (42.15)	189.7 (46.57)
CE CV	0.058 0.130 0.200	0.112 0.251 0.200	0.063 0.140 0.200	0.106 0.237 0.200	0.110 0.245 0.200
τ (sep, lung) [μm]	8.090 (1.487)	7.208 (1.117)	6.909 (1.191)	10.16 (0.7125)	8.306 (1.601)
CE CV	0.082 0.184 0.200	0.069 0.155 0.200	0.077 0.172 0.200	0.031 0.070 0.200	0.086 0.193 0.200
MLI (lung) [μm]	33.71 (2.165)	30.7 (2.510)	32.44 (5.317)	42.99 (4.328)	35.36 (2.124)
CE CV	0.029 0.064 0.200	0.037 0.082 0.200	0.073 0.164 0.200	0.045 0.101 0.200	0.027 0.060 0.250

Abbreviations: alv, alveoli; CE, coefficient of error; CV, coefficient of variation; MLI, mean linear intercept; N, alveoli number; N<sub>v</sub>, alveolar density; par, parenchyma; S, surface area; sep, septa; S<sub>v</sub>, surface density; V<sub>v</sub>, volume; V<sub>v</sub>, volume density; τ, arithmetic mean septal thickness. Values are presented as mean (SD, n = 5 lungs per group).

**TABLE 3** Structural parameters assessed for the lungs of mouse pups exposed to 85% O<sub>2</sub> hyperoxia for the first 14 days of postnatal life

Parameter	C57BL/6J mean (SD)	BALB/cJ mean (SD)	FVB/NJ mean (SD)	C3H/HeJ mean (SD)	DBA/2J mean (SD)								
V (lung) [cm <sup>3</sup> ]	0.2631 (0.04713)	0.3392 (0.02554)	0.2388 (0.03994)	0.3044 (0.06942)	0.2240 (0.04921)								
CE	CV	0.080	0.179	0.200	0.075	0.167	0.200	0.102	0.228	0.200	0.110	0.220	0.200
	CE <sup>2</sup> /CV <sup>2</sup>	0.9382 (0.0130)	0.9085 (0.0317)	0.9253 (0.0416)	0.8891 (0.0200)	0.9177 (0.0296)							
V <sub>v</sub> (par/lung) [%]	CV	0.006	0.014	0.200	0.016	0.035	0.200	0.020	0.045	0.200	0.010	0.022	0.200
	CE <sup>2</sup> /CV <sup>2</sup>	1.28 (0.205)	2.85 (0.251)	1.77 (0.101)	2.17 (0.512)	2.09 (0.541)							
N (alv, lung) 10 <sup>6</sup>	CV	0.072	0.160	0.200	0.039	0.088	0.199	0.026	0.057	0.202	0.106	0.236	0.200
	CE <sup>2</sup> /CV <sup>2</sup>	0.5304 (0.1047)	0.9279 (0.0692)	0.8157 (0.1160)	0.8003 (0.0915)	0.6665 (0.0981)							
N <sub>v</sub> (alv/par, lung) 10 <sup>7</sup> [cm <sup>-3</sup> ]	CV	0.088	0.197	0.200	0.033	0.075	0.200	0.064	0.142	0.200	0.051	0.114	0.200
	CE <sup>2</sup> /CV <sup>2</sup>	462.7 (23.74)	549.0 (34.08)	505.4 (42.94)	477.7 (38.95)	473.1 (85.6)							
S <sub>v</sub> (lung) [cm <sup>-1</sup> ]	CV	0.023	0.051	0.200	0.028	0.062	0.200	0.038	0.085	0.200	0.036	0.082	0.200
	CE <sup>2</sup> /CV <sup>2</sup>	114.3 (21.86)	169.3 (19.52)	110.9 (14.29)	130.5 (36.21)	147.0 (32.01)							
S (alv epi, lung) [cm <sup>2</sup> ]	CV	0.035	0.079	0.200	0.062	0.138	0.200	0.096	0.214	0.200	0.052	0.117	0.200
	CE <sup>2</sup> /CV <sup>2</sup>	10.54 (0.8286)	9.677 (1.332)	11.43 (2.448)	13.82 (1.622)	11.69 (3.262)							
τ (sep, lung) [μm]	CV	0.035	0.079	0.200	0.062	0.138	0.200	0.096	0.214	0.200	0.052	0.117	0.200
	CE <sup>2</sup> /CV <sup>2</sup>	65.55 (4.628)	53.73 (4.777)	56.72 (6.646)	56.59 (10.68)	63.62 (12.44)							
MLI (lung) [μm]	CV	0.032	0.071	0.200	0.040	0.089	0.200	0.052	0.117	0.200	0.084	0.189	0.200
	CE <sup>2</sup> /CV <sup>2</sup>	0.098	0.196	0.098	0.196	0.098	0.196	0.098	0.196	0.098	0.196	0.098	0.196

Abbreviations: alv, alveoli; CE, coefficient of error; CV, coefficient of variation; MLI, mean linear intercept; N, alveoli number; N<sub>v</sub>, alveolar density; par, parenchyma; S, surface area; sep, septa; S<sub>v</sub>, surface density; V, volume; V<sub>v</sub>, volume density; τ, arithmetic mean septal thickness.

Values are presented as mean (SD), n = 5 lungs per group for all groups, except for the DBA/2J group, where four lungs were assessed.

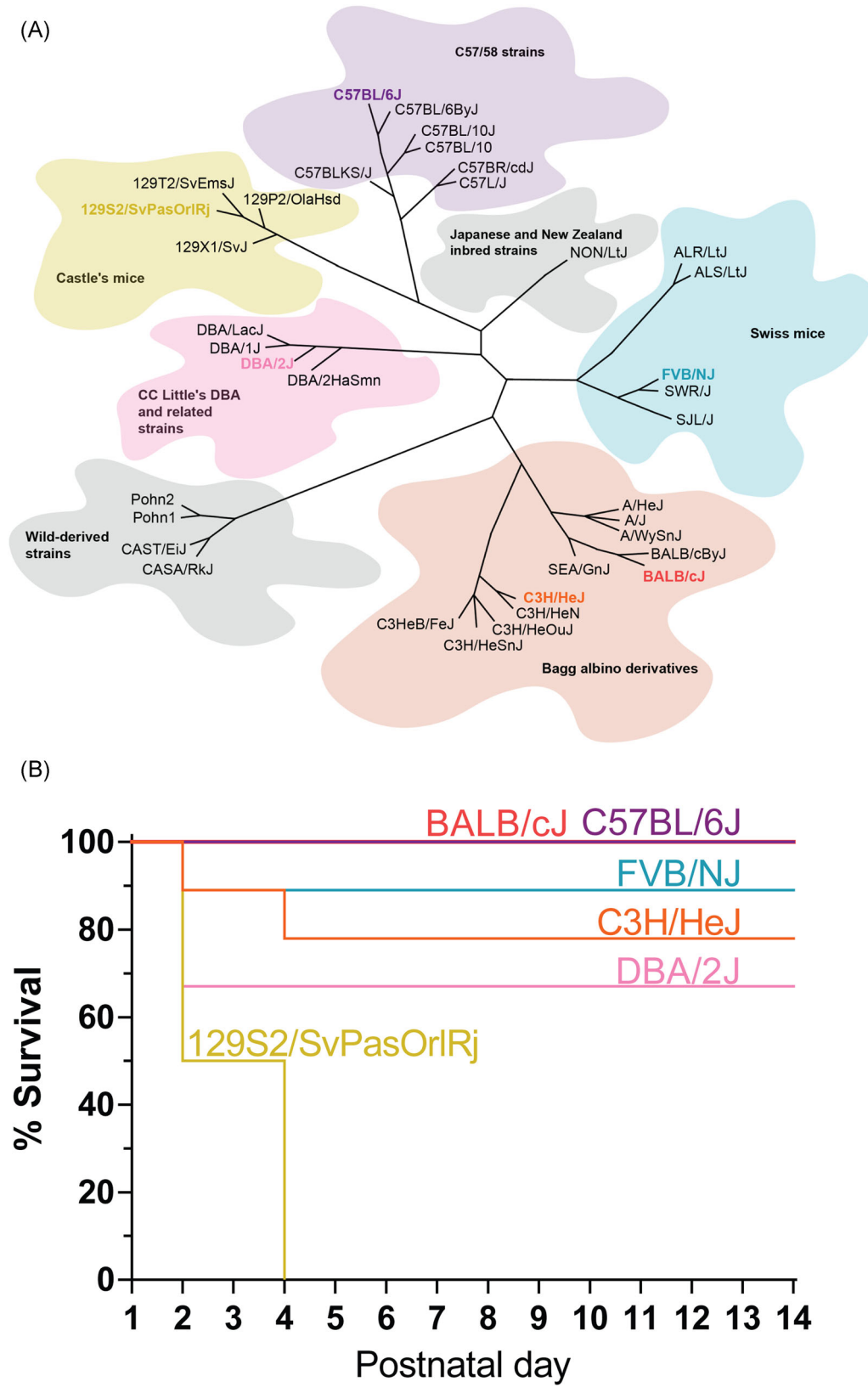
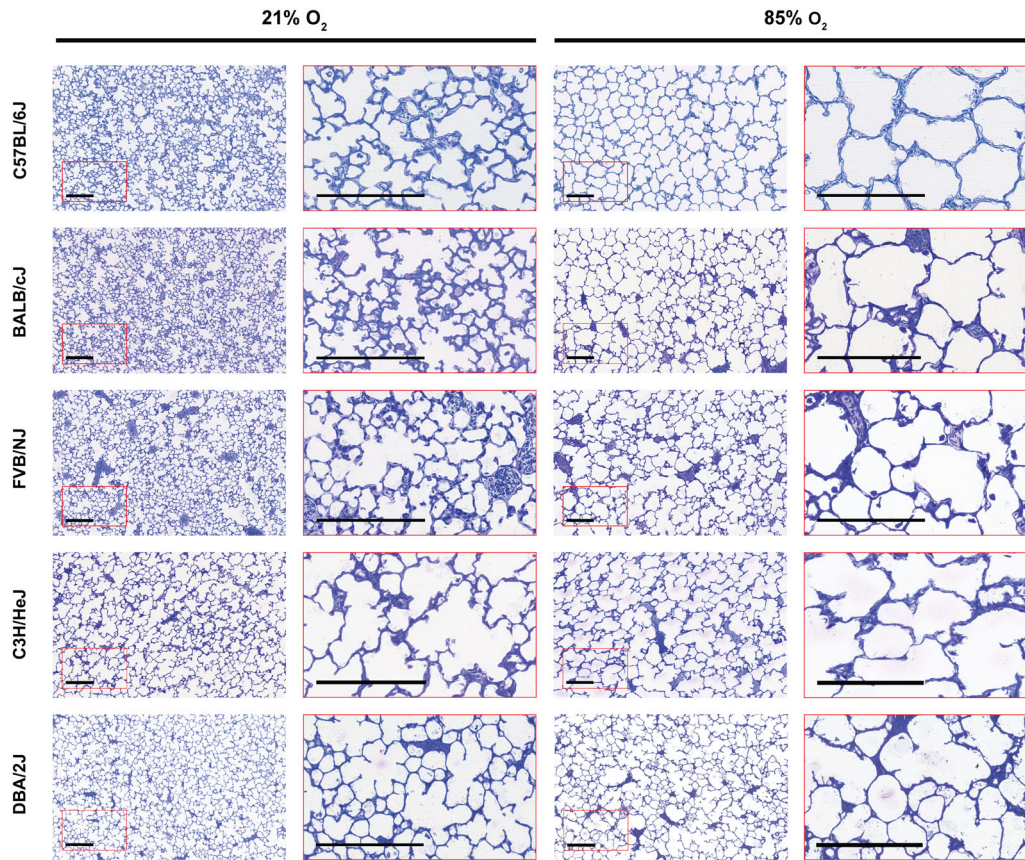


FIGURE 1 Continued.



**FIGURE 2** Strain-dependent perturbations to the development of the alveolar architecture in five inbred mouse strains. Representative Richardson-stained, plastic-embedded lung tissue sections are illustrated for C57BL/6J, BALB/cJ, FVB/NJ, C3H/HeJ, and DBA/2J mouse pups that were exposed to either 21% O<sub>2</sub> or 85% O<sub>2</sub> for the first 14 days of postnatal life, at which time-point lungs were harvested. Each section presented is representative of sections examined from five different mouse lungs for all strains and oxygen exposure conditions, except for the DBA/2J strain exposed to 85% O<sub>2</sub>, where the lungs of four mice were examined. The red box demarcates the area of a section presented at higher magnification in the image to the right of the respective section. Scale bar = 200 μm [Color figure can be viewed at wileyonlinelibrary.com]

(27.7%–51.5%; Figure 3A). These trends were supported by studies on alveolar density (Figure 3B), where C57BL/6J mouse pups exhibited the greatest reduction in alveolar density in response to hyperoxia exposure (64.8%), followed by BALB/cJ and FVB/NJ strains, which both exhibited a 46.6% to 47.4% decrease in alveolar density (Figure 3B). The C3H/HeJ and DBA/2J strains were least affected, exhibiting a 35.9% and 45.9% decrease in alveolar density, respectively, after hyperoxia exposure. With the exception of C57BL/6J mouse pups, hyperoxia exposure did not impact lung volume (Figure 3C).

Histopathological hallmarks of BPD include fewer and larger alveoli (“alveolar simplification”) with some suggestion that septa are also thicker in affected patients. Thus, arithmetic means septal

thickness (Figure 4A) and the MLI (Figure 4B) were also assessed. Septal thickness was increased in four of five strains after hyperoxia exposure, with the FVB/NJ strain exhibiting the largest magnitude (a 65.4% increase) and the C57BL/6J and BALB/cJ strains exhibiting the smallest magnitude (both with 30.3%–34.3% increase) of change in septal thickness (Figure 4A); whilst the DBA/2J strain was unaffected. While MLI often serves a surrogate of the approximate diameter of an alveolus, it is important to note that this is an oversimplification of the alveolar architecture, because alveoli are not spherical. All five strains examined exhibited an increased MLI after hyperoxia exposure, with C57BL/6J mouse pups exhibiting the greater increase (94.5%) in MLI after hyperoxia exposure (Figure 4B). Together, these data document

**FIGURE 1** Strain-dependent survival responses of mice to hyperoxia exposure in the postnatal period. A, Mouse strains were selected to be as genetically diverse as possible, and representative of commonly-used mouse strains in preclinical studies on bronchopulmonary dysplasia. Phylogenetic relatedness of mouse strains is based on the SNP analysis of Petkov et al,<sup>39</sup> from which the phylogenetic tree has been modified to indicate seven groups of inbred mice commonly used in experimental studies. The mouse strains used in this study are indicated in a colored font, which corresponds with the colors used to describe the mouse strains in the survival curve in the lower panel. B, Survival of mouse pups from six different inbred strains during hyperoxia (85% O<sub>2</sub>) exposure over the first 14 days of postnatal life (n = 9, per group; representing at least two litters per group). Note: the survival curve reflects either mice that were found dead or mice that were cannibalized in the cages. Under animal ethics guidelines, mice would have been euthanized when scored for distress or lack of condition. However, no mice were scored as being in distress or in poor condition before being found dead. SNP, single-nucleotide polymorphism [Color figure can be viewed at wileyonlinelibrary.com]

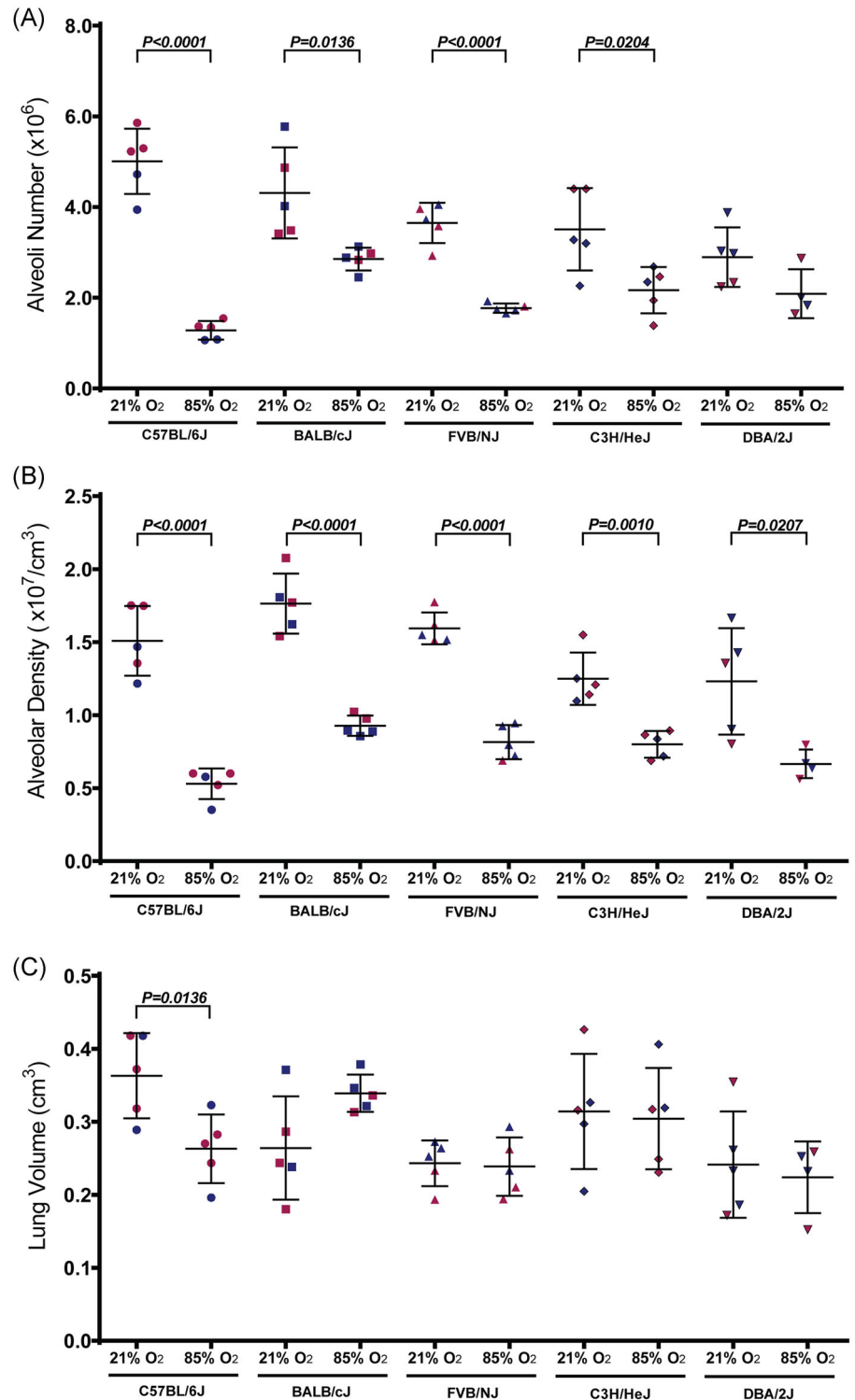


**FIGURE 3** Quantitative analysis of alveoli number and alveolar density by design-based stereology. A, Alveoli number, (B) alveolar density, and (C) lung volume were assessed in the lungs of mouse pups from five different inbred mouse strains on the 14th day of postnatal life, after exposure to either 21% O<sub>2</sub> or 85% O<sub>2</sub> for the first 14 days of postnatal life. Additional lung structure data and analyses of these data are provided in Table 2 and Table 3. Red symbols indicate female animals, whilst blue symbols indicate male animals. Data represent mean  $\pm$  SD ( $n = 5$  per group, except for hyperoxia-exposed DBA/2J, where  $n = 4$ ). Each data point represents an individual animal. Pairwise comparisons between 21% O<sub>2</sub>-exposed and 85% O<sub>2</sub>-exposed animals of the same strain were made by the unpaired Student *t* test. *P* values below 0.05 are indicated [Color figure can be viewed at [wileyonlinelibrary.com](http://wileyonlinelibrary.com)]

that hyperoxia exposure drove changes in the postnatal maturation of the lung architecture in all the five mouse strains investigated. The type and magnitude of these perturbations varied, depending on the mouse strain used. The C57BL/6J strain exhibited the greatest magnitude of effect in alveoli number, density, and MLI; whilst the FVB/NJ strain exhibited the greatest magnitude of increase in septal thickness.

### 4.3 | Hyperoxia effects on antioxidant pathways are strain dependent

Hyperoxia exposure causes appreciable oxidative stress in the developing mouse lung, which is likely to result in the engagement of the lung antioxidant response. Thus, the expression of key participants in lung antioxidant pathways was assessed by real-time

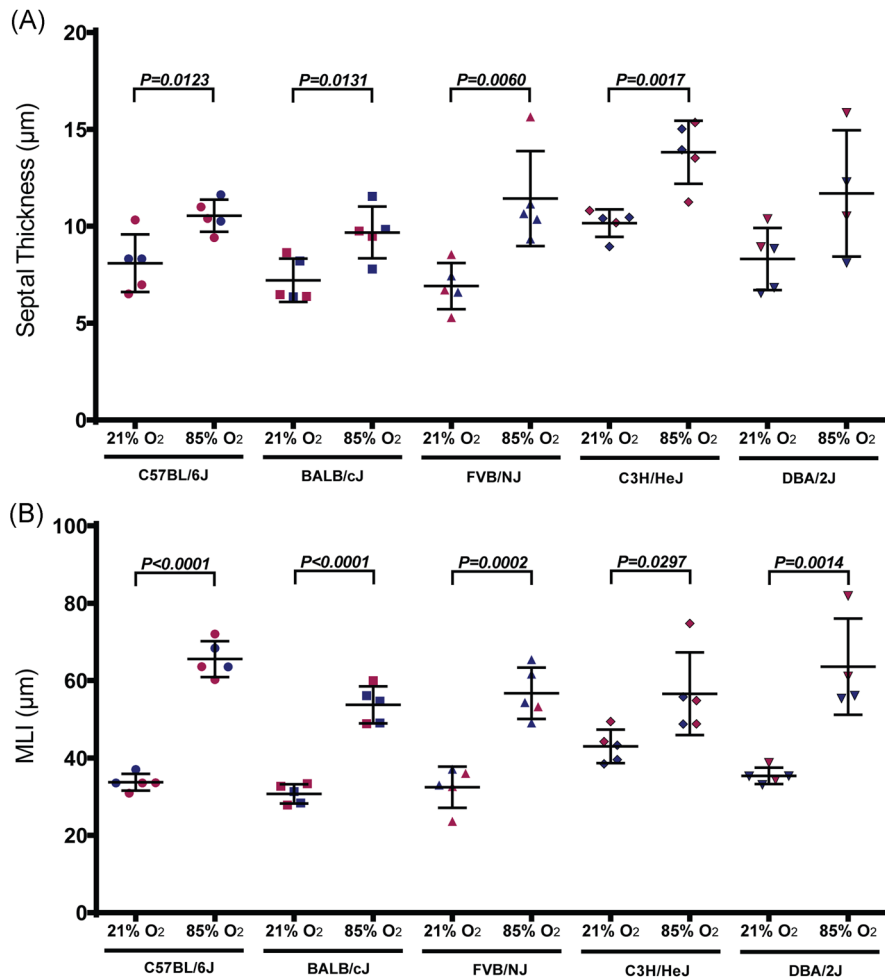


**FIGURE 4** Quantitative analysis of septal thickness and mean linear intercept by design-based stereology. A, Arithmetic mean septal thickness and (B) mean linear intercept (MLI) was assessed in the lungs of mouse pups from five different inbred mouse strains on the 14th day of postnatal life, after exposure to either 21% O<sub>2</sub> or 85% O<sub>2</sub> for the first 14 days of postnatal life. Additional lung structure data and analyses of these data are provided in Table 2 and Table 3. Red symbols indicate female animals, whilst blue symbols indicate male animals. Data represent mean  $\pm$  SD ( $n = 5$  per group, except for hyperoxia-exposed DBA/2J, where  $n = 4$ ). Each data point represents an individual animal. Pairwise comparisons between 21% O<sub>2</sub>-exposed and 85% O<sub>2</sub>-exposed animals of the same strain were made by the unpaired Student *t* test. *P* values below 0.05 are indicated [Color figure can be viewed at [wileyonlinelibrary.com](http://wileyonlinelibrary.com)]

RT-PCR, with expression changes validated for selected members by immunoblot. Using steady-state levels of SOD3 protein as an example, it is evident that the baseline (in mouse pups maintained under normoxic conditions) SOD3 protein steady-state levels varied considerably with mouse strain (Figure S2). Turning to the hyperoxia-based BPD model: a pronounced increase in steady-state levels of mRNA encoding SOD1 and SOD2 (Figure S3A and S3B), as well as SOD3 (Figure 5A), was noted in C57BL/6J mouse lungs after hyperoxia exposure. The *Sod1* steady-state mRNA levels were not influenced in other strains by hyperoxia exposure, whilst *Sod2* and *Sod3* steady-state mRNA levels were either increased or unchanged in other mouse strains. Changes in *Sod3* steady-state mRNA levels generally reflected in SOD3 protein levels assessed by immunoblot; although an increase in SOD3 steady-state protein levels (but not *Sod3* steady-state levels mRNA; Figure 5A) was also noted in hyperoxia-exposed BALB/cJ mouse pups (Figure 5B).

As with SOD, the expression of glutathione metabolizing enzymes in the lung was also impacted by hyperoxia exposure, where increased lung steady-state mRNA levels of *Gss* (encoding GSS) were noted in C57BL/6J, BALB/cJ, and DBA/2J strains (Figure 6A). These trends were largely validated by immunoblot (Figure 6B), where increased steady-state GSS levels were noted in hyperoxia-exposed mouse lungs from all five mouse strains.

Steady-state mRNA levels of *glutathione peroxidase 1* (encoding *GPx1*) were also noted in C57BL/6J, BALB/cJ, and FVB/NJ strains (Figure S4A), whilst steady-state mRNA levels of *glutathione disulfide reductase* (encoding *Gsr*) were largely unaffected by hyperoxia exposure (Figure S4B).

Other antioxidant enzyme families were also profiled. Steady-state mRNA levels of *thioredoxin 1* (encoding *Txn1*) were decreased by hyperoxia exposure in BALB/cJ and C3H/HeJ strains (Figure S5A). The C57BL/6J strain exhibited dramatically lower steady-state mRNA levels of *Txn1* compared with the other mouse strains (eg, 286-fold, compared with the BALB/cJ strain; Figure S5A). Lung steady-state mRNA levels of both *Txnrd1* and *Txnrd2*, which encode cytosolic and mitochondrial thioredoxin reductase (TXNRD) isozymes, respectively were stable (reflected by a  $\Delta C_t$  difference  $< 1$ ), except for the C57BL/6J strain, where increased *Txnrd1* and decreased *Txnrd2* steady-state mRNA levels were noted (Figure S6A and S6B). Steady-state mRNA levels of *Cat* (encoding catalase) were decreased by hyperoxia exposure in the C57BL/6J, BALB/cJ, and C3H/HeJ strains, with the greatest magnitude of decrease, noted in the C57BL/6J strain (Figure S5B). It is noteworthy that the C57BL/6J strain exhibited the highest steady-state mRNA levels of *Cat* under hyperoxic and normoxic conditions, compared with the other mouse strains (eg, 7.2-fold, compared with the BALB/cJ strain; Figure S5B).

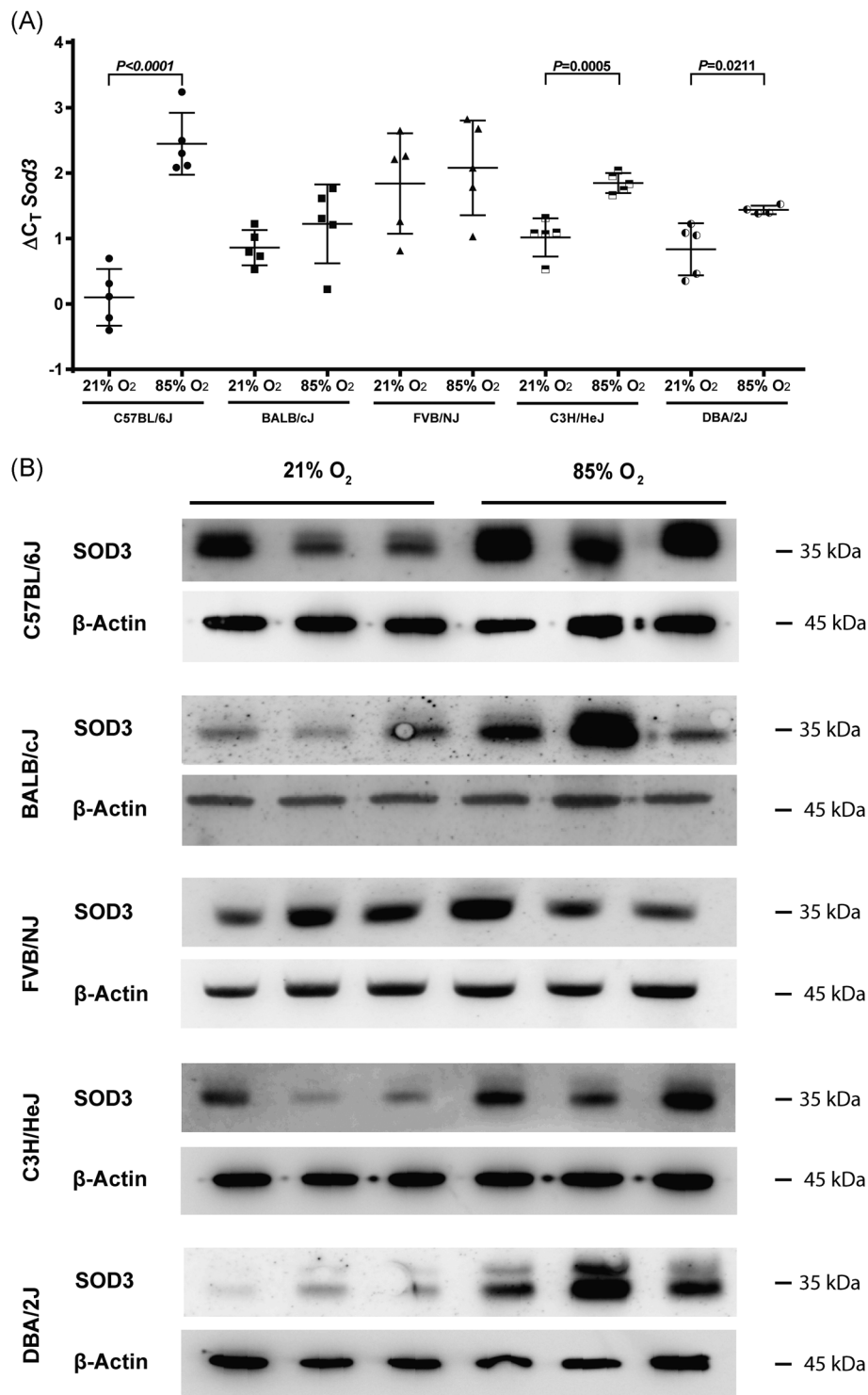


**FIGURE 5** Expression of superoxide dismutase 3 in five different inbred mouse strains exposed to hyperoxia. A, Steady-state levels of *Sod3* mRNA were assessed in the lungs of mouse pups from five different inbred mouse strains on the 14th day of postnatal life, after exposure to either 21% O<sub>2</sub> or 85% O<sub>2</sub> for the first 14 days of postnatal life, using the primers described in Table 1. Data reflect mean  $\Delta C_T \pm$  SD ( $n = 5$  per group, except for hyperoxia-exposed DBA/2J, where  $n = 4$ ). Pairwise comparisons between 21% O<sub>2</sub>-exposed and 85% O<sub>2</sub>-exposed animals of the same strain were made by the unpaired Student *t* test. *P* values below 0.05 are indicated. B, Steady-state SOD3 protein levels were assessed in the lungs of mouse pups from five different inbred mouse strains on the 14th day of postnatal life, after exposure to either 21% O<sub>2</sub> or 85% O<sub>2</sub> for the first 14 days of postnatal life; using steady-state  $\beta$ -actin levels to demonstrate loading equivalence. Immunoreactive bands are presented for three different 21% O<sub>2</sub>-exposed animals alongside bands from three different 85% O<sub>2</sub>-exposed animals. The full uncropped blots are presented in Figure S1A. mRNA, messenger RNA; SOD3, superoxide dismutase 3

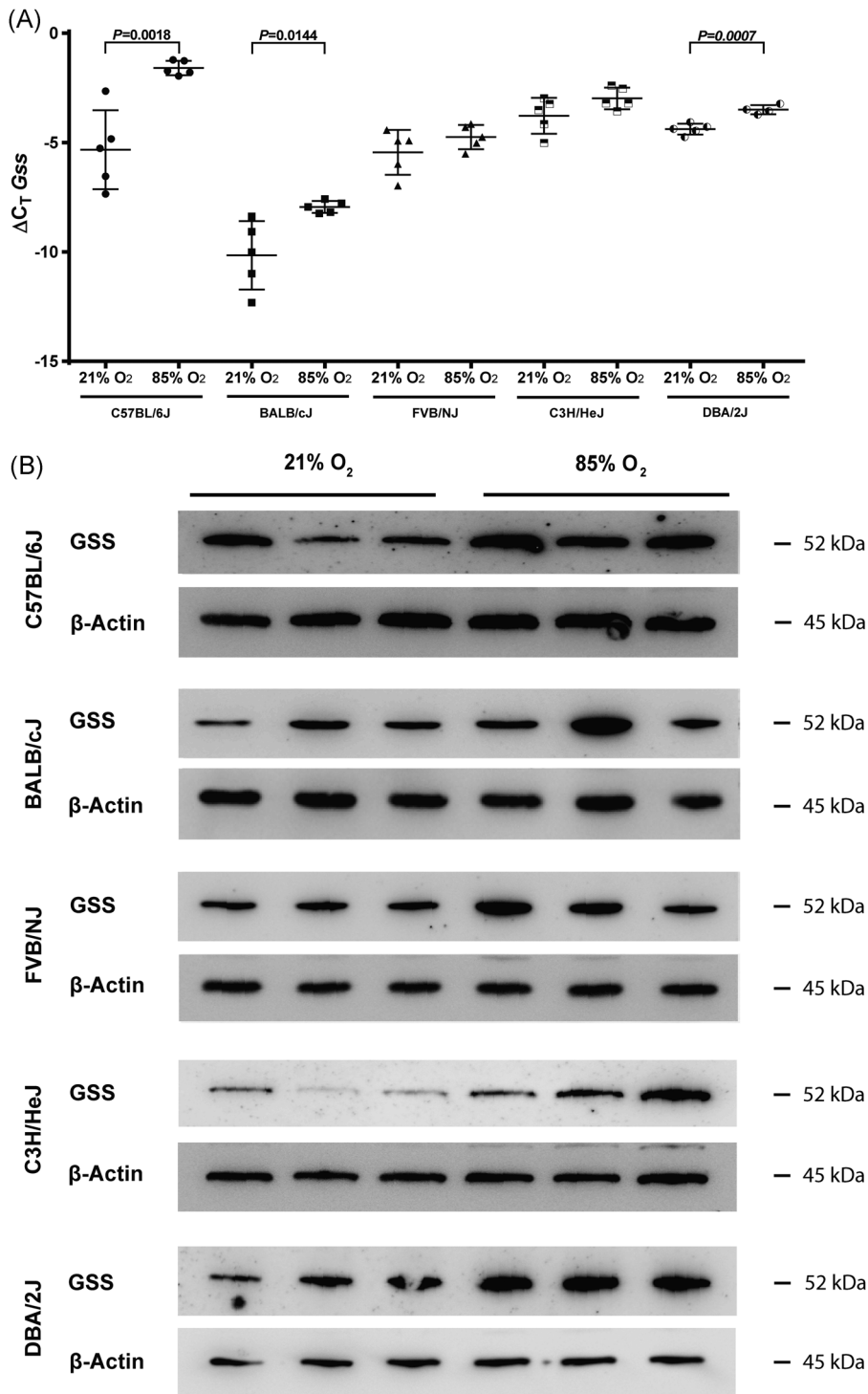


**FIGURE 6** Expression of glutathione synthetase in five different inbred mouse strains exposed to hyperoxia. A, Steady-state levels of *Gss* mRNA were assessed in the lungs of mouse pups from five different inbred mouse strains on the 14th day of postnatal life, after exposure to either 21% O<sub>2</sub> or 85% O<sub>2</sub> for the first 14 days of postnatal life, using the primers described in Table 1. Data reflect mean  $\Delta C_t \pm$  SD ( $n = 5$  per group, except for hyperoxia-exposed DBA/2J, where  $n = 4$ ). Pairwise comparisons between 21% O<sub>2</sub>-exposed and 85% O<sub>2</sub>-exposed animals of the same strain were made by the unpaired Student *t* test. *P* values below 0.05 are indicated. B, Steady-state GSS protein levels were assessed in the lungs of mouse pups from five different inbred mouse strains on the 14th day of postnatal life, after exposure to either 21% O<sub>2</sub> or 85% O<sub>2</sub> for the first 14 days of postnatal life; using steady-state  $\beta$ -actin levels to demonstrate loading equivalence. Immunoreactive bands are presented for three different 21% O<sub>2</sub>-exposed animals alongside bands from three different 85% O<sub>2</sub>-exposed animals. The full uncropped blots are presented in Figure S1B. Gss, glutathione synthetase; mRNA, messenger RNA

Nuclear factor (erythroid-derived 2)-like 2 (NFE2L2, also called NRF2) is a transcription factor that regulates the expression of many antioxidant proteins.<sup>40,41</sup> Under normoxic conditions, the C57BL/6J strain exhibited the highest and the DBA/2J strain the lowest *Nfe2l2* steady-state mRNA levels (4.34-fold change difference; Figure 7A). Hyperoxia exposure reduced *Nfe2l2* steady-state mRNA levels in the C57BL/6J and BALB/cJ strains, with the C57BL/6J strain exhibiting the greatest magnitude of change (Figure 7A).

Of the six-member peroxiredoxin (PRDX) family, steady-state mRNA levels of *Prdx1* were decreased in the C57BL/6J, BALB/cJ, and FVB/NJ strains (Figure 7B) after hyperoxia exposure; whilst those of *Prdx6* were increased in the C57BL/6J and BALB/cJ strains (Figure 7C). Steady-state mRNA levels of *Prdx2*, *Prdx3*, and *Prdx4* were unchanged in all strains (Figure S7A and S7C) after hyperoxia exposure. Steady-state mRNA levels of *Prdx5* were increased by hyperoxia in the BALB/cJ and DBA/2J strains, where the C57BL/6J strain stood out as having the

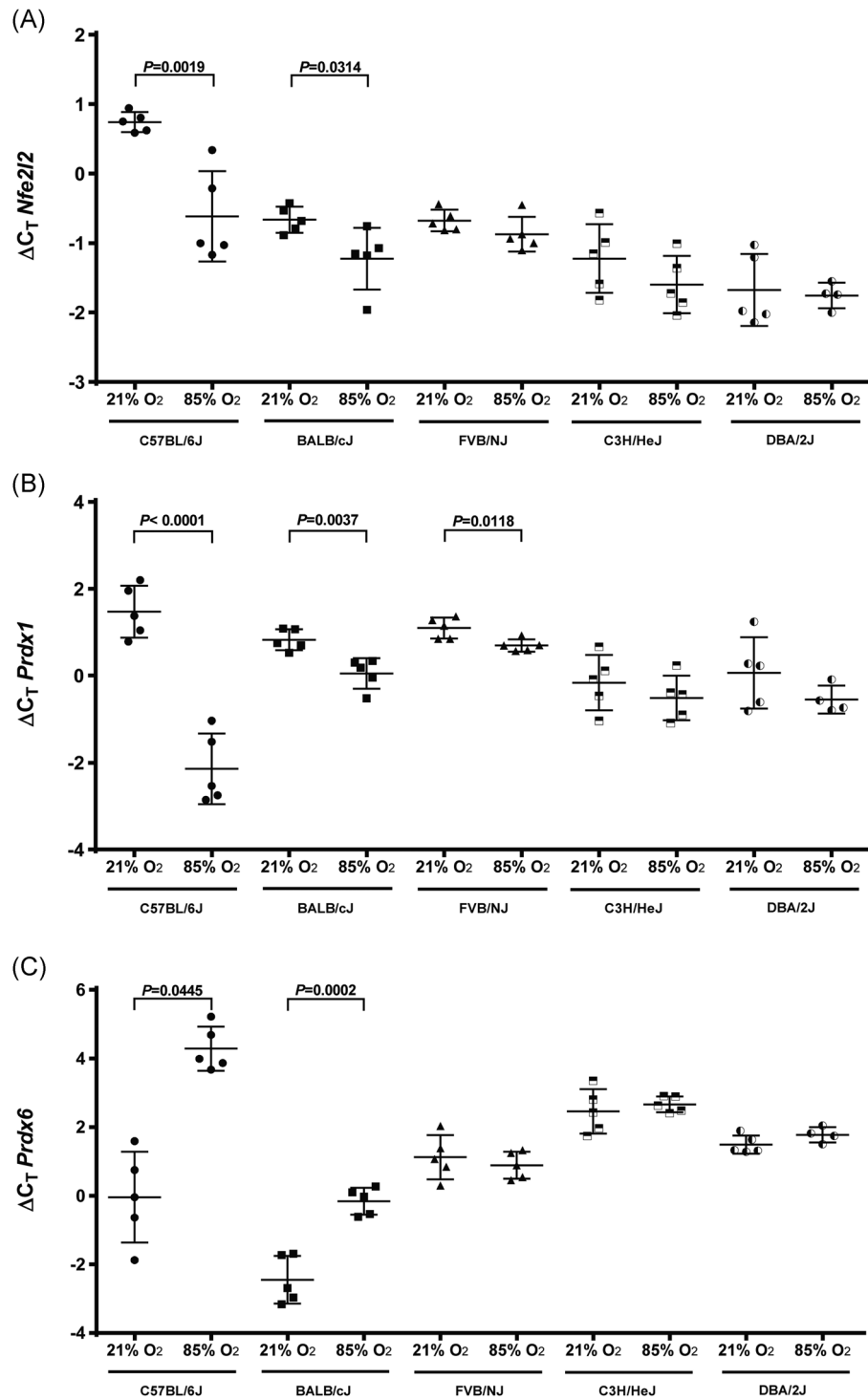


**FIGURE 7** Expression of nuclear factor (erythroid-derived 2)-like 2, peroxiredoxin 1 and peroxiredoxin 6 in five different inbred mouse strains exposed to hyperoxia. Steady-state mRNA levels of (A) *Nfe2l2* (encoding nuclear factor [erythroid-derived 2]-like 2; also called *Nrf2*), (B) *Prdx1* (encoding peroxiredoxin 1), and (C) *Prdx6* (encoding peroxiredoxin 6) were assessed in the lungs of mouse pups from five different inbred mouse strains on the 14th day of postnatal life, after exposure to either 21% O<sub>2</sub> or 85% O<sub>2</sub> for the first 14 days of postnatal life, using the primers described in Table 1. Data reflect mean  $\Delta C_T \pm$  SD (n = 5 per group, except for hyperoxia-exposed DBA/2J, where n = 4). Pairwise comparisons between 21% O<sub>2</sub>-exposed and 85% O<sub>2</sub>-exposed animals of the same strain were made by the unpaired Student t test. P values below 0.05 are indicated. mRNA, messenger RNA

lowest baseline steady-state mRNA levels of *Prdx5* compared with the other mouse strains (eg, 21.3-fold, compared with the BALB/cJ strain; Figure S8A). Steady-state levels mRNA levels of *Hmox1*, which encodes heme oxygenase-1, were highest in C57BL/6J mice under hyperoxic and normoxic conditions, compared with the other mouse strains investigated (Figure S8B), but *Hmox1* levels were unchanged by hyperoxia exposure in any strain, with the exception of a moderate reduction in the BALB/cJ strain (Figure S8B). Of the paraoxonase (PON) group, steady-state mRNA levels for *Pon1*, *Pon2*, and *Pon3* were all increased in the DBA/2J strain (Figure S9A and S9C), where increased *Pon2* steady-state mRNA levels were also noted for C57BL/6J and BALB/cJ strains (Figure S9B).

## 5 | DISCUSSION

The laboratory mouse is the most widely used experimental animal in preclinical models of BPD.<sup>19,42</sup> Studies to date have used a broad spectrum of mouse strains—and thus, genetic backgrounds—for these studies,<sup>19,43</sup> which raises concerns about the broader translational relevance of conclusions drawn about disease pathogenesis and preclinical therapeutics that are based on the studies conducted with a single mouse strain. In addition, comparisons between related studies reported in the literature may be complicated by strain differences. For example, two studies on the impact of periostin on hyperoxia-induced perturbations to lung alveolarization have revealed either no impact<sup>44</sup> or a dramatic impact<sup>45</sup> of periostin; where mouse strain was one of the several variables distinguishing the two studies. More recent studies have revealed that the mouse strain plays a key role in the evaluation of potentially useful pharmacological interventions in preclinical mouse models, where the utility of aurothioglucose to limit hyperoxia-induced stunting of lung alveolarization was supported using the C3H/HeN mouse strain but not the C57BL/6J mouse strain.<sup>28</sup> These studies highlight the importance of considering and accurately reporting the mouse strains used in experimental studies, and also, highlight a need for a side-by-side comparison of the impact of mouse strain on lung development in hyperoxia-based BPD models.

To this end, we set out to perform a systematic comparison of hyperoxia-induced perturbations to postnatal lung maturation in six widely used strains of the laboratory mouse. The mouse strains were selected from five of the seven groups described in the laboratory mouse strain family tree that was based on 1638 informative single-nucleotide polymorphisms, which were compared in 106 inbred mouse strains<sup>39</sup> (Figure 1A). Of these, the C3H/HeJ and BALB/cJ strains are both from the Bagg albino-derived group, although present on divergent branches of this group; the FVB/NJ strain is from the Swiss mouse group, the C57BL/6J strain is from the general C57/C58 group, the 129S2/SvPasOrIRj is derived from the members of the Castle group, and the DBA/2J strain is from C.C. Little's DBA and related strain group. No mice were selected from Japan and New Zealand inbred strains group, or from the wild-derived strain group, as no strains within these groups are generally used in preclinical

BPD models. Newborn mouse pups were randomized to litters of four or five pups per litter, to match the generally smaller litter sizes of the DBA/2J strain, which did not appreciably skew the sex balance (compare male and female animals in Figures 3 and 4).

Nursing 129S2/SvPasOrIRj dams maintained under hyperoxic conditions were noticeably agitated, being aggressive when provoked (when hands were placed into the cage), vocal (squeaking), and noted outside of the nest, in contrast to nursing 129S2/SvPasOrIRj dams maintained under normoxic conditions, who were generally observed cohabiting the nest with pups. All pups from all litters were lost by P4, with the pup corpses found partially consumed, without any prior indication of morbidity (although all 129S2/SvPasOrIRj litters maintained under normoxic conditions were unaffected). The cause of death was not determined. As such, the 129S2/SvPasOrIRj strain was not considered further. The 129S-derived strains often form part of a mixed strain background in transgenic studies, hence their inclusion here. The remaining five strains survived hyperoxia to P14.

Considering normally developing mice maintained under normoxic conditions: of the five mouse strains examined at 2 weeks of postnatal age, the C57BL/6J strain exhibited the largest number of alveoli, and the highest lung volume; whilst the DBA/2J strain exhibited the smallest number of alveoli and the lowest lung volume. Other strain differences in normally developing mice included the arithmetic mean septal thickness, which was highest in the C3H/HeJ strain and was lowest in the FVB/NJ strain. To our knowledge, these data have not been previously reported. Using MLI as a rough surrogate for the average diameter of an alveolus, visual inspection of lung tissue section revealed that the C3H/HeJ strain had the largest alveoli, which has been previously reported (using morphometry; in comparison with C57BL/6J and A/J mouse strains),<sup>46</sup> with BALB/cJ mice having the smallest MLI. Given the baseline differences in the expression of antioxidants in normally developing mouse lungs, it remains interesting to assess whether the differences in antioxidant expression may be (at least in part) responsible for the differences in lung structure in normally developing mice, noted above.

It is generally accepted that, for a mouse model to appreciably mimic the histopathological changes to the lung parenchyma that occur in infants with BPD, alveolar simplification must occur, which includes observation of fewer, larger alveoli with thickened septa.<sup>19</sup> Given changes in lung volume between strains and hyperoxia exposure, alveolar density represents the best measure of lung alveolarization. Turning to the hyperoxia-based mouse model of BPD: hyperoxia exposure most effectively stunted lung alveolarization in the C57BL/6J strain (64.8% reduction in alveolar density), whilst the C3H/HeJ was least affected (35.9% reduction in alveolar density). This trend was preserved considering the impact of hyperoxia on the size of alveoli (using the MLI as a surrogate for alveoli diameter), where hyperoxia exerted the most pronounced impact on MLI in the C57BL/6J strain (94.5% increase) and the least pronounced impact on the C3H/HeJ strain (31.6% increase). These differences are also noted in septal thickness, where hyperoxia exposure resulted in a 65.4% increase in septal thickness in the FVB/NJ strain (representing the largest increase), compared with the smallest effect noted in the

C57BL/6J strain (30.3% increase). As such, there is tremendous variation in the susceptibility of the lungs of different mouse strains to hyperoxia-driven effects on alveolarization. It is important to acknowledge that the data reported here, and the interpretations of those data, concern a single window of hyperoxia exposure (the first 14 days of postnatal life), and additional time courses of hyperoxia exposure might suggest that time is an important variable in how different strains respond to hyperoxia.

The authors do acknowledge that the term susceptibility may mean different things to different people. Here, susceptibility is defined as an intrinsic predisposition of a mouse strain to hyperoxia-driven alterations to the development of the lung structure: either generation of new alveoli or the progressive thinning of the septa, which are both components of the postnatal maturation of the lung. Our data clarify that while hyperoxia did impact lung alveolarization in all five mouse strains examined; the same injurious stimulus (always 85% O<sub>2</sub> for the first 14 postnatal days of life) provoked different patterns of damage (considering both the nature and the magnitude of the damage) in different mouse strains. Thus, we concluded that the five different mouse strains had different intrinsic susceptibility to oxygen toxicity in the postnatal period.

The C57BL/6J strain appeared to be the most severely impacted strain in terms of alveoli number and size after hyperoxia exposure in the postnatal period. It is likely that hyperoxia exposure, which generates appreciable oxidative stress would engage the antioxidant machinery of the developing lung. We speculated that more susceptible strains might display a different expression profile of the antioxidant machinery; or that more susceptible strains would be unable to effectively engage the antioxidant machinery of the lungs after hyperoxic insult. To this end, the gene and, in selected instances, protein expression of a broad spectrum of participants in lung antioxidant programs were profiled. It should be noted at this junction that changes in steady-state mRNA levels are not always predictive of changes in steady-state protein levels, as has been demonstrated, for example, for lung adenocarcinomas.<sup>47</sup>

SOD, which play key roles in antioxidant defenses of living cells exposed to oxygen, by catalyzing the dismutation of the O<sub>2</sub><sup>-</sup> radical, have received attention as possible modulators of the impact of hyperoxia on lung alveolarization, with SOD3 confirmed as being protective,<sup>48</sup> whilst SOD2 appeared to have no function in this regard in mice,<sup>49</sup> although increased expression of lung SOD2 in a baboon model of BPD has been described.<sup>50</sup> This idea is consistent with SOD3 being upregulated in hyperoxia-exposed mouse lungs.

Both the C57BL/6J, and to a lesser degree, the BALB/cJ strain, also effectively increased the expression of glutathione metabolizing enzymes, such as GSS and GPX1, but not glutathione disulfide reductase, after hyperoxia exposure. This is potentially important because disturbances to glutathione dynamics have been noted in hyperoxia-exposed newborn rat lungs,<sup>51</sup> although the role of the glutathione metabolizing machinery in aberrantly developing immature lungs remains unclear. To date, genetic ablation of *Gpx1*, one of six GPX enzymes, was without impact on lung alveolarization in the hyperoxia-based animal model of BPD,<sup>52</sup> possibly due to

compensation by other isozymes. Similarly, overexpression of glutathione reductase in alveolar type II cells in adult mice did not protect against hyperoxic lung injury,<sup>53</sup> although that study did not address lung alveolarization in neonates. Thus, the consequence of upregulated *Gss* and *Gpx1* expression in the lung after hyperoxia exposure awaits experimental clarification.

Atypical antioxidants were also considered in this study, including the three-member PON family, which are an emerging but poorly understood group of antioxidants, with PON2 accredited with broad antioxidant and cell protective effects.<sup>54</sup> Interestingly, the DBA/2J strain upregulated *Pon1*, *Pon2*, and *Pon3* expression in response to hyperoxia exposure, whilst the C57BL/6J and BALB/cJ strain upregulated *Pon2* expression. A role for *Pon2* in arrested alveolarization has yet to be addressed experimentally.

Thioredoxin (*Txn1*) exerts antioxidant activity through facilitating reduction of other proteins by cysteine thiol-disulfide exchange and has received much attention in preclinical BPD models,<sup>55,56</sup> together with two TXNRD isozymes.<sup>28,57,58</sup> Inhibition of TXNRD with aurothioglucose attenuated the impact of hyperoxia on lung alveolarization, ostensibly through sustained activation of NFE2L2, which is a key regulator of antioxidant activity in the lung.<sup>59,60</sup> Interestingly, and pertinent to this study, this effect was mouse strain dependent, where aurothioglucose was effective only in the C3H/HeN and not in the C57BL/6 strain.<sup>28</sup> Data presented here indicate that the C57BL/6J has 5.2-fold higher *Txnrd1* baseline steady-state mRNA levels than does the C3H/HeJ strain, and the C3H/HeJ strain has 155-fold higher *Txn1* baseline steady-state mRNA levels than does the C57BL/6J strain. Also important is that hyperoxia exposure decreased the steady-state mRNA levels of *Txn1* in the C3H/HeJ strain, but not in the C57BL/6J strain; whilst conversely, hyperoxia exposure decreased steady-state mRNA levels of *Txnrd1* in the C57BL/6J strain, but not in the C3H/HeJ strain. It is tempting to speculate that the vastly different baseline levels of *Txn1* and *Txnrd1* in these two mouse strains, and the strain-dependent impact of hyperoxia on *Txn1* and *Txnrd1* expression, may—at least in part—explain the strain-dependent effects of aurothioglucose in the preclinical BPD model. Along these lines, it is also noteworthy that steady-state *Nfe2l2* mRNA levels were decreased by hyperoxia exposure in the C57BL/6J strain, but not the C3H/HeJ strain.

Taken together, the data presented here document a spectrum of—at times unpredictable—differences in strain-dependent responses of isogenic (inbred) mouse strains to hyperoxia, in the context of postnatal lung maturation. This raises the question of whether it might be instructive to rather employ outbred mouse strains in studies on hyperoxia-driven perturbations to lung development, to appropriately account for the background genetic variation present in any patient with BPD cohort. Indeed, one recent study<sup>61</sup> has identified outbred mice are being as phenotypically stable (for experimental studies) as are inbred mice; and at the same time, outbred mice provide an experimental system that might offer better reproducibility, because the system is more resistant to environmental differences and experimental conditions. Returning to inbred mice, studies on the pathology and pathogenesis of experimental BPD in higher vertebrates

employing preterm baboons<sup>62</sup> or preterm lambs<sup>63</sup> may be instructive in guiding the choice of inbred mouse strain by investigators.

Genetic mouse models have often failed to demonstrate a close link between antioxidants and lung disease.<sup>64</sup> Because lung alveolarization in the C57BL/6J strain was the most severely impacted by hyperoxia exposure of any mouse strain, it is noteworthy that the C57BL/6J strain was also most effective at upregulating the expression of a very large spectrum of antioxidants (*Sod1*, *Sod2*, *Sod3*, *Gss*, *Gpx*, *Pon2*, *Txnrd2*, and *Prdx6*): more so than any other strain. This observation warrants speculation about whether the extensive engagement of the antioxidant machinery may have also had a deleterious impact on mouse lung alveolarization. Furthermore, the C57BL/6J strain, and to a lesser degree, the BALB/cJ strain stood out as exhibiting a pronounced downregulation of the expression of genes encoding other components of lung antioxidant systems (*Cat*, *Txnrd1*, and *Prdx1*) in response to hyperoxia exposure. It would be interesting to experimentally assess whether any of these three antioxidants play a particularly pivotal role in the response of the developing mouse lung to hyperoxia exposure.

## 6 | CONCLUSION

The genetic backgrounds of the C57BL/6, BALB/c, A/J, C3H/He, FVB/N, and DBA/2 laboratory mouse strains defines the response of the developing mouse lungs to hyperoxic insults used in preclinical models of BPD. These responses are different, with alveolar density and size being most affected by hyperoxia exposure in C57BL/6J strain, whilst septal thickness was most impacted by hyperoxia exposure in the FVB/NJ strain. Components of the lung antioxidant machinery were expressed at different baseline levels in different mouse strains, and this expression was influenced differently by hyperoxia exposure in different mouse strains. This may account—at least in part—for the strain-dependent differences noted in the effects of hyperoxia exposure on lung alveolarization.

## ACKNOWLEDGMENTS

This study was supported by the Max Planck Society; Rhön Klinikum AG grant FI\_66; University Hospital Giessen and Marburg grant UKGM62589135; the Federal Ministry of Higher Education, Research and the Arts of the State of Hessen “LOEWE Program”, the German Center for Lung Research (*Deutsches Zentrum für Lungenforschung*), and by the German Research Foundation (*Deutsche Forschungsgemeinschaft*) through Excellence Cluster EXC147, Collaborative Research Center SFB1213/1 (project A03), Clinical Research Unit KFO309/1 (projects P2, P5, P6, and P8), and individual research grant Mo 1789/1.

## ORCID

Rory E Morty  <http://orcid.org/0000-0003-0833-9749>

## REFERENCES

- Northway WH, Jr., Rosan RC, Porter DY. Pulmonary disease following respirator therapy of hyaline-membrane disease. Bronchopulmonary dysplasia. *N Engl J Med*. 1967;276(7):357-368.
- Jobe AH, Steinhorn R. Can we define bronchopulmonary dysplasia? *J Pediatr*. 2017;188:19-23.
- Voynow JA. “New” bronchopulmonary dysplasia and chronic lung disease. *Paediatr Respir Rev*. 2017;24:17-18.
- Abman SH. Medical progress series: bronchopulmonary dysplasia at 50 years—an introduction. *J Pediatr*. 2017;188:18-18.
- Alvira CM, Morty RE. Can we understand the pathobiology of bronchopulmonary dysplasia? *J Pediatr*. 2017;190:27-37.
- Saugstad OD. Oxygen and oxidative stress in bronchopulmonary dysplasia. *J Perinat Med*. 2010;38(6):571-577.
- Carraro S, Filippone M, Da Dalt L, et al. Bronchopulmonary dysplasia: the earliest and perhaps the longest lasting obstructive lung disease in humans. *Early Hum Dev*. 2013;89(suppl 3):S3-S5.
- Bhattacharya S, Zhou Z, Yee M, et al. The genome-wide transcriptional response to neonatal hyperoxia identifies *Ahr* as a key regulator. *Am J Physiol Lung Cell Mol Physiol*. 2014;307(7):L516-L523.
- Morrow LA, Wagner BD, Ingram DA, et al. Antenatal determinants of bronchopulmonary dysplasia and late respiratory disease in preterm infants. *Am J Respir Crit Care Med*. 2017;196(3):364-374.
- Aschner JL, Bancalari EH, McEvoy CT. Can we prevent bronchopulmonary dysplasia? *J Pediatr*. 2017;189:26-30.
- Greenough A, Ahmed N. Perinatal prevention of bronchopulmonary dysplasia. *J Perinat Med*. 2013;41(1):119-126.
- Shahzad T, Radajewski S, Chao CM, Bellusci S, Ehrhardt H. Pathogenesis of bronchopulmonary dysplasia: when inflammation meets organ development. *Mol Cell Pediatr*. 2016;3(1):23.
- Yu KH, Li J, Snyder M, Shaw GM, O’Brodivich HM. The genetic predisposition to bronchopulmonary dysplasia. *Curr Opin Pediatr*. 2016;28(3):318-323.
- Collins JJP, Tibboel D, de Kleer IM, Reiss IKM, Rottier RJ. The future of bronchopulmonary dysplasia: emerging pathophysiological concepts and potential new avenues of treatment. *Front Med (Lausanne)*. 2017;4:61.
- Surate Solaligue DE, Rodríguez-Castillo JA, Ahlbrecht K, Morty RE. Recent advances in our understanding of the mechanisms of late lung development and bronchopulmonary dysplasia. *Am J Physiol Lung Cell Mol Physiol*. 2017;313(6):L1101-L1153.
- Bao EL, Chytsiakova A, Brahmajothi MV, et al. Bronchopulmonary dysplasia impairs L-type amino acid transporter-1 expression in human and baboon lung. *Pediatr Pulmonol*. 2016;51(10):1048-1056.
- Berger J, Bhandari V. Animal models of bronchopulmonary dysplasia. The term mouse models. *Am J Physiol Lung Cell Mol Physiol*. 2014;307(12):L936-L947.
- O’Reilly M, Thébaud B. Animal models of bronchopulmonary dysplasia. The term rat models. *Am J Physiol Lung Cell Mol Physiol*. 2014;307(12):L948-L958.
- Nardiello C, Mižiková I, Morty RE. Looking ahead: where to next for animal models of bronchopulmonary dysplasia? *Cell Tissue Res*. 2017;367(3):457-468.
- Ehrhardt H, Pritze T, Oak P, et al. Absence of TNF- $\alpha$  enhances inflammatory response in the newborn lung undergoing mechanical ventilation. *Am J Physiol Lung Cell Mol Physiol*. 2016;310(10):L909-L918.
- Nardiello C, Mižiková I, Silva DM, et al. Standardisation of oxygen exposure in the development of mouse models for bronchopulmonary dysplasia. *Dis Model Mech*. 2017;10(2):185-196.
- Beauchemin KJ, Wells JM, Kho AT, et al. Temporal dynamics of the developing lung transcriptome in three common inbred strains of laboratory mice reveals multiple stages of postnatal alveolar development. *PeerJ*. 2016;4:e2318.
- Nichols JL, Gladwell W, Verhein KC, et al. Genome-wide association mapping of acute lung injury in neonatal inbred mice. *FASEB J*. 2014;28(6):2538-2550.

24. Cho HY, Jedlicka AE, Reddy SP, Zhang LY, Kensler TW, Kleeberger SR. Linkage analysis of susceptibility to hyperoxia. *Nrf2* is a candidate gene. *Am J Respir Cell Mol Biol*. 2002;26(1):42-51.
25. Hudak BB, Zhang LY, Kleeberger SR. Inter-strain variation in susceptibility to hyperoxic injury of murine airways. *Pharmacogenetics*. 1993;3(3):135-143.
26. Whitehead GS, Burch LH, Berman KG, Piantadosi CA, Schwartz DA. Genetic basis of murine responses to hyperoxia-induced lung injury. *Immunogenetics*. 2006;58(10):793-804.
27. Lajko M, Cardona HJ, Taylor JM, Farrow KN, Fawzi AA. Photoreceptor oxidative stress in hyperoxia-induced proliferative retinopathy accelerates rd8 degeneration. *PLoS One*. 2017;12(7):e0180384.
28. Li Q, Li R, Wall SB, et al. Aurothioglucose does not improve alveolarization or elicit sustained *Nrf2* activation in C57BL/6 models of bronchopulmonary dysplasia. *Am J Physiol Lung Cell Mol Physiol*. 2018;314(5):L736-L742.
29. Rath P, Nardiello C, Surate Solaligue DE, et al. Caffeine administration modulates TGF- $\beta$  signaling but does not attenuate blunted alveolarization in a hyperoxia-based mouse model of bronchopulmonary dysplasia. *Pediatr Res*. 2017;81(5):795-805.
30. Mižiková I, Pfeffer T, Nardiello C, et al. Targeting transglutaminase 2 partially restores extracellular matrix structure but not alveolar architecture in experimental bronchopulmonary dysplasia. *FEBS J*. 2018;285(16):3056-3076.
31. Hsia CC, Hyde DM, Ochs M, Weibel ER, ATS/ERS Joint Task Force on Quantitative Assessment of Lung Structure. An official research policy statement of the American Thoracic Society/European Respiratory Society: standards for quantitative assessment of lung structure. *Am J Respir Crit Care Med*. 2010;181(4):394-418.
32. Hoang TV, Nardiello C, Surate Solaligue DE, et al. Stereological analysis of individual lung lobes during normal and aberrant mouse lung alveolarisation. *J Anat*. 2018;232(3):472-484.
33. Pozarska A, Rodríguez-Castillo JA, Surate Solaligue DE, et al. Stereological monitoring of mouse lung alveolarization from the early postnatal period to adulthood. *Am J Physiol Lung Cell Mol Physiol*. 2017;312(6):L882-L895.
34. Schneider JP, Ochs M. Alterations of mouse lung tissue dimensions during processing for morphometry: a comparison of methods. *Am J Physiol Lung Cell Mol Physiol*. 2014;306(4):L341-L350.
35. Michel RP, Cruz-Orive LM. Application of the Cavalieri principle and vertical sections method to lung: estimation of volume and pleural surface area. *J Microsc*. 1988;150(Pt 2):117-136.
36. Richardson KC, Jarett L, Finke EH. Embedding in epoxy resins for ultrathin sectioning in electron microscopy. *Stain Technol*. 1960;35:313-323.
37. Mižiková I, Palumbo F, Tábi T, et al. Perturbations to lysyl oxidase expression broadly influence the transcriptome of lung fibroblasts. *Physiol Genomics*. 2017;49(8):416-429.
38. Lambert JF, Benoit BO, Colvin GA, Carlson J, Delville Y, Quesenberry PJ. Quick sex determination of mouse fetuses. *J Neurosci Methods*. 2000;95(2):127-132.
39. Petkov PM, Ding Y, Cassell MA, et al. An efficient SNP system for mouse genome scanning and elucidating strain relationships. *Genome Res*. 2004;14(9):1806-1811.
40. Biswas SK, Rahman I. Environmental toxicity, redox signaling and lung inflammation: the role of glutathione. *Mol Aspects Med*. 2009;30(1-2):60-76.
41. Cho HY, Reddy SP, Kleeberger SR. *Nrf2* defends the lung from oxidative stress. *Antioxid Redox Signal*. 2006;8(1-2):76-87.
42. Ambalavanan N, Morty RE. Searching for better animal models of BPD: A perspective. *Am J Physiol Lung Cell Mol Physiol*. 2016;311(5):L924-L927.
43. Silva DM, Nardiello C, Pozarska A, Morty RE. Recent advances in the mechanisms of lung alveolarization and the pathogenesis of bronchopulmonary dysplasia. *Am J Physiol Lung Cell Mol Physiol*. 2015;309(11):L1239-L1272.
44. Ahlfeld SK, Gao Y, Wang J, et al. Periostin downregulation is an early marker of inhibited neonatal murine lung alveolar septation. *Birth Defects Res A Clin Mol Teratol*. 2013;97(6):373-385.
45. Bozyk PD, Bentley JK, Popova AP, et al. Neonatal periostin knockout mice are protected from hyperoxia-induced alveolar simplification. *PLoS One*. 2012;7(2):e31336.
46. Soutiere SE, Tankersley CG, Mitzner W. Differences in alveolar size in inbred mouse strains. *Respir Physiol Neurobiol*. 2004;140(3):283-291.
47. Chen G, Gharib TG, Huang CC, et al. Discordant protein and mRNA expression in lung adenocarcinomas. *Mol Cell Proteomics*. 2002;1(4):304-313.
48. Delaney C, Wright RH, Tang JR, et al. Lack of EC-SOD worsens alveolar and vascular development in a neonatal mouse model of bleomycin-induced bronchopulmonary dysplasia and pulmonary hypertension. *Pediatr Res*. 2015;78(6):634-640.
49. Gupta A, Perez M, Lee KJ, Taylor JM, Farrow KN. SOD2 activity is not impacted by hyperoxia in murine neonatal pulmonary artery smooth muscle cells and mice. *Int J Mol Sci*. 2015;16(3):6373-6390.
50. Clerch LB, Wright AE, Coalson JJ. Lung manganese superoxide dismutase protein expression increases in the baboon model of bronchopulmonary dysplasia and is regulated at a posttranscriptional level. *Pediatr Res*. 1996;39(2):253-258.
51. Kennedy KA, Lane NL. Effect of *in vivo* hyperoxia on the glutathione system in neonatal rat lung. *Exp Lung Res*. 1994;20(1):73-83.
52. Bouch S, O'Reilly M, de Haan JB, Harding R, Sozo F. Does lack of glutathione peroxidase 1 gene expression exacerbate lung injury induced by neonatal hyperoxia in mice? *Am J Physiol Lung Cell Mol Physiol*. 2017;313(1):L115-L125.
53. Heyob KM, Rogers LK, Welty SE. Glutathione reductase targeted to type II cells does not protect mice from hyperoxic lung injury. *Am J Respir Cell Mol Biol*. 2008;39(6):683-688.
54. Ng CJ, Wadleigh DJ, Gangopadhyay A, et al. Paraoxonase-2 is a ubiquitously expressed protein with antioxidant properties and is capable of preventing cell-mediated oxidative modification of low density lipoprotein. *J Biol Chem*. 2001;276(48):44444-44449.
55. Tipple TE. The thioredoxin system in neonatal lung disease. *Antioxid Redox Signal*. 2014;21(13):1916-1925.
56. Tipple TE, Welty SE, Nelin LD, Hansen JM, Rogers LK. Alterations of the thioredoxin system by hyperoxia: implications for alveolar development. *Am J Respir Cell Mol Biol*. 2009;41(5):612-619.
57. Li Q, Wall SB, Ren C, et al. Thioredoxin reductase inhibition attenuates neonatal hyperoxic lung injury and enhances nuclear factor E2-related factor 2 activation. *Am J Respir Cell Mol Biol*. 2016;55(3):419-428.
58. Dunigan K, Li Q, Li R, Locy ML, Wall SB, Tipple TE. The thioredoxin reductase inhibitor auranofin induces heme oxygenase-1 in lung epithelial cells via *Nrf2*-dependent mechanisms. *Am J Physiol Lung Cell Mol Physiol*. 2018;315:L545-L552.
59. Cho HY, van Houten B, Wang X, et al. Targeted deletion of *nrf2* impairs lung development and oxidant injury in neonatal mice. *Antioxid Redox Signal*. 2012;17(8):1066-1082.
60. McGrath-Morrow SA, Lauer T, Collaco JM, et al. Transcriptional responses of neonatal mouse lung to hyperoxia by *Nrf2* status. *Cytokine*. 2014;65(1):4-9.
61. Tuttle AH, Philip VM, Chesler EJ, Mogil JS. Comparing phenotypic variation between inbred and outbred mice. *Nat Methods*. 2018;15(12):994-996.
62. Yoder BA, Coalson JJ. Animal models of bronchopulmonary dysplasia. The preterm baboon models. *Am J Physiol Lung Cell Mol Physiol*. 2014;307(12):L970-L977.
63. Albertine KH. Utility of large-animal models of BPD: chronically ventilated preterm lambs. *Am J Physiol Lung Cell Mol Physiol*. 2015;308(10):L983-L1001.

64. Ho YS. Transgenic and knockout models for studying the role of lung antioxidant enzymes in defense against hyperoxia. *Am J Respir Crit Care Med.* 2002;166(12 Pt 2):S51-S56.

## SUPPORTING INFORMATION

Additional supporting information may be found online in the Supporting Information section at the end of the article.

**How to cite this article:** Tiono J, Surate Solaligue DE, Mižíková I, et al. Mouse genetic background impacts susceptibility to hyperoxia-driven perturbations to lung maturation. *Pediatric Pulmonology.* 2019;1-18.

<https://doi.org/10.1002/ppul.24304>